IOP Publishing | Institute of Physics and Engineering in Medicine Physics in Medicine & Biology

Phys. Med. Biol. **61** (2016) 1705–1721 doi:10.1088/0031-9155/61/4/1705

# Analytical calculation of proton linear energy transfer in voxelized geometries including secondary protons

**D Sanchez-Parcerisa[1,4], M A Cortés-Giraldo[2], D Dolney[1], M Kondrla[1], M Fager[1,3] and A Carabe[1]**

[1] Department of Radiation Oncology, Hospital of the University of Pennsylvania, Philadelphia, PA 19104, USA
[2] Department of Atomic, Molecular and Nuclear Physics, Universidad de Sevilla, Spain
[3] Department of Physics and Astronomy, University of Pennsylvania, Philadelphia, PA 19104, USA

E-mail: daniel@nuclear.fis.ucm.es and a.carabe@uphs.upenn.edu

Received 3 August 2015, revised 22 December 2015
Accepted for publication 5 January 2016
Published 3 February 2016


**Abstract**

In order to integrate radiobiological modelling with clinical treatment planning for proton radiotherapy, we extended our in-house treatment planning system FoCa with a 3D analytical algorithm to calculate linear energy transfer (LET) in voxelized patient geometries. Both active scanning and passive scattering delivery modalities are supported. The analytical calculation is much faster than the Monte-Carlo (MC) method and it can be implemented in the inverse treatment planning optimization suite, allowing us to create LET-based objectives in inverse planning.

The LET was calculated by combining a 1D analytical approach including a novel correction for secondary protons with pencil-beam type LET-kernels. Then, these LET kernels were inserted into the proton-convolution-superposition algorithm in FoCa. The analytical LET distributions were benchmarked against MC simulations carried out in Geant4. A cohort of simple phantom and patient plans representing a wide variety of sites (prostate, lung, brain, head and neck) was selected.

The calculation algorithm was able to reproduce the MC LET to within 6% (1 standard deviation) for low-LET areas (under 1.7 keV $\mu m^{-1}$) and within 22% for the high-LET areas above that threshold. The dose and LET distributions can be further extended, using radiobiological models, to include

[4] Author to whom any correspondence should be addressed.
Current address: Department of Atomic, Molecular and Nuclear Physics, Universidad Complutense de Madrid, Spain.

 © 2016 Institute of Physics and Engineering in Medicine Printed in the UK 

radiobiological effectiveness (RBE) calculations in the treatment planning system. This implementation also allows for radiobiological optimization of treatments by including RBE-weighted dose constraints in the inverse treatment planning process.

Keywords: protontherapy, linear energy transfer, LET, particle therapy, RBE, radiobiology, proton therapy

(Some figures may appear in colour only in the online journal)

## 1. Introduction

While the radiobiological effects on tissues of proton radiotherapy fields depend primarily on their absorbed dose distribution, a finer analysis leads to the introduction of the concept of radiobiological effectiveness (RBE), defined as the ratio of the absorbed dose of the reference radiation ($^{60}$Co gamma rays) and the dose given by a specific radiation type which produces the same biological effect. The RBE depends on multiple factors (Paganetti 2014), including dose, LET, choice of endpoint and cell line. LET, which is defined as the average energy deposited locally per unit path length by electronic collisions, is the major descriptor of the biological damage to cells at the microscopic level (Kraft and Kramer 2013). While variations of LET within proton fields have been correlated with observable biological effects (Paganetti 2012, Carabe *et al* 2013), the lack of reliable data, combined with substantial uncertainties and computational difficulties, have led the medical community to adopt a fixed, LET-independent value for the proton RBE of 1.1 (Paganetti 2014). However, this does not mean that radiobiological optimization with protons is not possible: LET itself can be used as a predictor for radiobiological outcome at the microscopic level, which would justify the use of purely LET-based objectives in treatment plan optimization. Additionally, phenomenological models exist that derive RBE from dose, LET and other parameters (Carabe-Fernandez *et al* 2007, Wedenberg *et al* 2013, McNamara *et al* 2015). These two approaches would directly benefit from a direct and fast method for calculating LET in clinical proton fields.

The most widespread method of calculating linear energy transfer in protontherapy fields is via Monte Carlo simulation (Grassberger and Paganetti 2011, Romano *et al* 2014, Cortés-Giraldo and Carabe 2015, Granville and Sawakuchi 2015) using generic particle transport codes. While capable of producing very accurate results, the long execution times of these Monte Carlo codes makes it difficult to incorporate them into daily clinical practice, or to use them to create LET-based objectives for inverse planning optimization. Also, and despite some successful attempts at measuring LET or LET-related quantities using silicon microdosimeters (Rosenfeld *et al* 2000, Wroe *et al* 2009, Rollet *et al* 2011, Guardiola *et al* 2015) and tissue-equivalent proportional counters (Kase *et al* 2012, Pérez-Andujar *et al* 2012), *in vivo* LET dosimetry is still far from daily clinical practice. Therefore, an accurate modelling of proton linear energy transfer is vital for implementing LET-painting strategies in a clinical setup (Giantsoudi *et al* 2013, Fager *et al* 2015). Such a model, based on a 1D formulation for primary protons only, was developed by Wilkens and Oelfke (2003), and later, its application to broad beams in 3D geometries was briefly discussed (Wilkens and Oelfke 2004). However, even though these models have been around for over ten years, no detailed uncertainty analysis has been published (that we are aware of).

The purpose of the article is two-fold. First, it presents an empirical correction for LET caused by secondary protons, which has a non-negligible effect in the entrance channel and represents an improvement over existing models. And second, it assesses the validity of

existing and refined analytical LET models, providing the 'error bars' for them from the most honest possible perspective. We revisit the Wilkens and Oelfke formulation, add a correction to account for the effect of secondary protons, combine it with a convolution-superposition dose calculation algorithm for pencil beams (Schaffner 2008, Ulmer and Schaffner 2011) and incorporate it into our in-house proton treatment planning system (TPS) FoCa (Sanchez-Parcerisa *et al* 2014a). The resulting LET distributions are compared against Monte Carlo simulations carried out with Geant4. The goal of this work is not to deliver a final, fully-functional proton LET model that can replace Monte Carlo simulations in all cases, but to quantify the uncertainties of the currently available models, identifying their error sources, and to explore the usability of analytical LET calculation in proton treatment planning in the context of a full TPS. Additionally, as a usage example of the LET model, RBE and RBE-weighted dose calculations for several patients are presented, using the newly published, phenomenological RBE model by McNamara *et al* (2015).

## 2. Materials and methods

### *2.1. Incorporating LET scoring into FoCa*

The ICRU, in their Technical Report 60 (ICRU 1998), defines LET in a restricted form $L_{\Delta}$, where delta electrons with an energy above the threshold $\Delta$ are not included. Most calculations in the literature (Wilkens and Oelfke 2003, Grassberger *et al* 2011, Romano *et al* 2014) use the unrestricted definition of LET, where LET corresponds to collision stopping power, assuming charged particle equilibrium (Grassberger and Paganetti 2011). While this definition of LET can be applied to a single particle, in which case its value is directly obtained from the stopping power tables, LET is often used to characterize complex radiation fields. There are two ways of averaging LET over all particles in a given radiation field: the track-averaged LET ($\mathrm{LET_t}$) and the dose-averaged LET ($\mathrm{LET_d}$), the latter being the more common of the two. However, with higher LET radiation such as carbon ion beams, the reduced number of particle tracks might make $\mathrm{LET_t}$ a more representative predictor of radiobiological effects (Romano *et al* 2014), but this does not seem to be the case for proton therapy. Thus, all references to LET existing in this article refer to dose-weighted LET.

A generic formulation of dose-averaged LET at a 3D point $z$ can be expressed as

$$\overline{\mathrm{LET_d}}(z) = \frac{\sum_i \int_0^{\infty} S_i^2(E)\varphi_E^i(z)\mathrm{d}E}{\sum_i \int_0^{\infty} S_i(E)\varphi_E^i(z)\mathrm{d}E}, \tag{1}$$

where the numerator and the denominator represent the sum, for all particle species $i$, of the product of its electronic stopping power $S_i$ multiplied by the local fluence spectra of species $i$ with energy $E$, integrated to over all energies. Because our initial model contains only primary protons, we can drop the summation terms and apply the classical Wilkens and Oelfke (2003) formulation, where numerator and denominator of expression (1) are restricted to primary protons and named $\langle S^2\rangle$ and $\langle S\rangle$ respectively, expressing the local LET at point z as $\langle S^2\rangle_z/\langle S\rangle_z$. The key of this analytical formulation is to approximate the proton local energy spectra by a Gaussian distribution around the mean residual range at each position, which is in turn determined by the classical Bortfeld formula (Bortfeld 1997) of $r = AE^p$, with $r$ the range and $E$ the nominal proton energy. In our implementation, the parameters $A$ and $p$, as well as the local energy spread of the beam (sigma) are determined from the FoCa physics models

(Sanchez-Parcerisa *et al* 2014a); in particular, new data was generated with our Monte Carlo code (detailed in section 2.2) and used to commission a new machine in FoCa to achieve agreement between the two methods. To avoid the singularity as E → 0, Wilkens and Oelfke (2003) proposed a regularization of the stopping power included in the LET formulation, expressing it in terms of the residual range rather than the remaining energy, so that $S(E)$ in equation (1) is substituted by $\overline{S_R(r)}$, expressed as

$$S_R(r) = \frac{1}{R}\int_r^{r+R} S(r')\mathrm{d}r', \tag{2}$$

where the d$E$ element is transformed into a d$r$ element using the Bortfeld formula. We used this approach to calculate our LET kernels, with a regularization parameter of $R = 35$ $\mu$m for best agreement with Monte Carlo data, chosen using a similar approach as described by Wilkens and Oelfke (2003) but, unlike in the original formulation, we performed the integration of the local energy spectra via numerical integration (using Matlab native function *integral*). Due to the sensitivity of this type of calculation to the choice of stopping power tables (Paul and Sánchez-Parcerisa 2013), we implemented tables generated by Geant4 in FoCa, to minimize the sources of discrepancy between FoCa and Monte Carlo at time of validation.

The power of the $\langle S^2\rangle/\langle S\rangle$ formulation is that, while $\mathrm{LET_d}$ is not an additive quantity, its components $\langle S^2\rangle$ and $\langle S\rangle$ are indeed additive quantities, which facilitates the calculation of the total LET distributions from different beams. A similar result could be obtained by simply adding up the final LET contributions from each beam weighted by their final dose; however, in the dose calculation are included other components (secondaries, recoils) for which the LET model would no longer hold, so that formulation would be somehow inconsistent. Therefore, we implemented $\langle S^2\rangle$ and $\langle S\rangle$ kernels in the FoCa dose calculation architecture (Sanchez-Parcerisa *et al* 2014a), mimicking the dose calculation with a convolution-superposition algorithm, for each of the individual components of the LET expression, and we completed the process by adding a final step in which the $\langle S^2\rangle$ and $\langle S\rangle$ distributions from all fields were combined to create a single LET distribution for all points with a non-negligible dose. All LET calculation classes were incorporated into the FoCa architecture via inheritance from similar dose calculation classes.

### *2.2. Empirical correction for LET of secondary protons*

Secondary protons, originated in nuclear interactions along the path of the primary beam, tend to have a lower energy than the protons that produce them and are ejected in all directions. Therefore, they increase the dose-weighted LET across the complete field, by a factor than can be up to 50% in the central axis and up to 200% in the penumbra (Grassberger and Paganetti 2011). In order to include the effect of these secondary protons in our model, we derived an empirical correction from Monte Carlo calculations (see details in section 2.3). We studied the absolute difference in LET between simulations accounting for all protons, and simulations accounting only for primary protons. In order to keep the correction to one dimension, we focused our study on the laterally-integrated LET curves. We fitted the ΔLET curves (Total LET–LET from primary protons only) for five different proton energies (ranges of 10 to 22 cm) to a 4th-order polynomial as a function of the relative residual range, and we then fitted the resulting coefficients to 3rd-order polynomials as a function of the beam nominal energy. Contrarily to other authors (Marsolat *et al* 2015), we did not incorporate any spot-size effects into the model, as its observed effect on the integrated LET curves was significantly lower than the dependence with the beam energy.

The ΔLET correction is then given by

**Table 1.** $p_{ij}$ coefficients for the ΔLET correction.

| $p_{ij}$ | $j=0$ | $j=1$ | $j=2$ | $j=3$ |
|---|---|---|---|---|
| $i=0$ | 0.3755 | −0.0809 | 0.005 554 | −0.000 1149 |
| $i=1$ | −3.925 | 1.036 | −0.061 77 | 0.001 221 |
| $i=2$ | 15.58 | −3.668 | 0.2162 | −0.004 250 |
| $i=3$ | −22.47 | 5.024 | −0.2927 | 0.005 736 |
| $i=4$ | 10.56 | −2.315 | 0.1332 | −0.002 601 |

$$\Delta\mathrm{LET} = \sum_{i=0}^{4} p_i(R_0)x^i \tag{3}$$

where $x = R_{\mathrm{res}}/R_0$ is the relative residual range, being $R_0$ the nominal range, and the coefficients $p_i$ are calculated from the nominal range using the formula $p_i = \sum_{j=0}^{3} p_{ij}{R_0}^i$, where $R_0$ is expressed in cm. The $p_{ij}$ coefficients implemented in our model are given in table 1.

We incorporated the ΔLET correction into the $\langle S^2\rangle$ kernel, using an effective kernel $\langle S^2\rangle_{\mathrm{eff}}$ throughout all the LET calculations. The total LET is thus calculated as $\mathrm{LET}_{\mathrm{total}} = \mathrm{LET}_{\mathrm{primary}} + \Delta\mathrm{LET} = \langle S^2\rangle/\langle S\rangle + \Delta\mathrm{LET} = [\langle S^2\rangle + \Delta\mathrm{LET}\cdot\langle S\rangle]/\langle S\rangle$, from which we define $\langle S^2\rangle_{\mathrm{eff}} = \langle S^2\rangle + \Delta\mathrm{LET}\cdot\langle S\rangle$.

### 2.3. Verification in Geant4

We incorporated the scoring method *C* as defined by Cortes-Giraldo and Carabe (2015) into *an* in-house Geant4 (Agostinelli *et al* 2003) model of the IBA proton therapy nozzles (Dolney *et al* 2013, Sanchez-Parcerisa *et al* 2014b), using version v9.4 (Patch-01) of Geant4 transport code with the physics list from Jarlskog and Paganetti (2008). In this scoring method, the dose-average LET at a voxel placed at point z, assuming that the voxel is crossed by *N* protons, with each proton taking $S_n$ steps within the voxel, is calculated as

$$\overline{\mathrm{LET_d}}(z) = \frac{\sum_{n=1}^{N}\sum_{s=1}^{S_n} \omega_n\, L_{sn}\, \varepsilon_{sn}}{\sum_{n=1}^{N}\sum_{s=1}^{S_n} \omega_n\, \varepsilon_{sn}}, \tag{4}$$

where $\varepsilon_{sn}$ is the electronic energy loss by the proton $n$ at step $s$, $\omega_n$ is the statistical weight of the proton $n$ and $L_{sn}$ is the *expected* electronic stopping power computed from Geant4 lookup tables according to the average kinetic energy of the step, which was calculated as the mean value between the kinetic energy values at the initial and final step points. The average kinetic energy was used to avoid bias on the computed LET value at voxels near the Bragg Peak, where the LET gradient is high compared to other regions. Also, steps which terminated due to an inelastic hadronic interaction were not considered because in this particular case the original proton track is terminated and thus the kinetic energy value at the final step point is considered as zero. This scoring method, using the *expected* electronic stopping power instead of the *real* LET calculated directly from the step done by the simulated proton, provides a dose-averaged LET estimator which has been confirmed to be stable to voxel size changes (Granville and Sawakuchi 2015) and values for the production threshold of secondary particles, which has been shown to have a non-negligible impact in similar scoring problems (Sánchez-Parcerisa *et al*

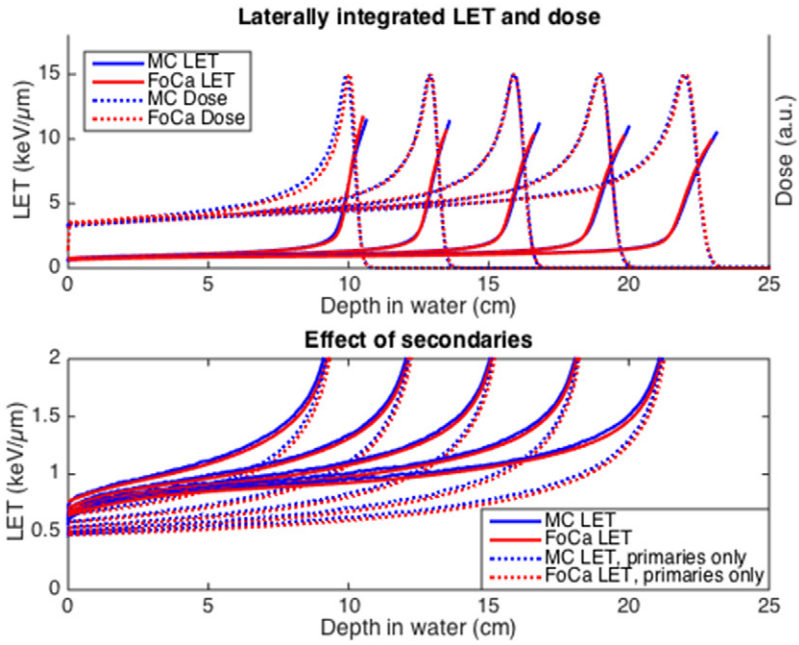


**Figure 1.** Top: depth dose and LET distributions, calculated with Monte Carlo and FoCa, for monoenergetic proton beams with ranges of 10 cm, 13 cm, 16 cm, 19 cm and 22 cm. Bottom: detail of upper figure for LET range under 2 keV $\mu$m$^{-1}$, showing the LET calculated with and without secondary protons (in Monte Carlo) and with and without secondary proton correction (in FoCa), for the five monoenergetic beams.

2012). Furthermore, this method has been observed to produce the most consistent results with respect to microdosimetry estimations (Cortés-Giraldo and Carabe 2015).

### *2.4. Derivation of phenomenological RBE distributions*

In order to assess the effects of the dose and LET distributions in a combined fashion, we calculated the RBE and RBE-weighted dose distributions using the phenomenological model by McNamara *et al* (2015), given by

$$\mathrm{RBE} = -\frac{1}{2D}\left(\frac{\alpha}{\beta}\right) + \frac{1}{D}\sqrt{\frac{1}{4}\left(\frac{\alpha}{\beta}\right)^2 + \left(0.991 + \frac{0.356}{\alpha/\beta}L\right)\left(\frac{\alpha}{\beta}\right)D + \left(1.101 - 0.0039\sqrt{\frac{\alpha}{\beta}}\,L\right)D^2}, \tag{5}$$

where $L$ and $D$ are the LET and dose per fraction distributions. We chose to use the recently published model by McNamara *et al* (2015) over the Carabe-Fernandez *et al* (2007) and Wedenberg (2013) models, since their derivation uses a quite comprehensive set of proton RBE experimental data. For our calculation, we used a prescribed biological dose per fraction of 1.8 Gy(RBE) for all cases, corresponding to a physical dose of 1.8/1.1 = 1.64 Gy. The $\alpha/\beta$ ratios were chosen at 3 Gy for normal tissues and 10 Gy for tumoral tissues (Kehwar and Sharma 2003), except for the prostate tumor, with an alpha/beta ratio of 1.5 Gy (Dasu and Toma-Dasu 2012).

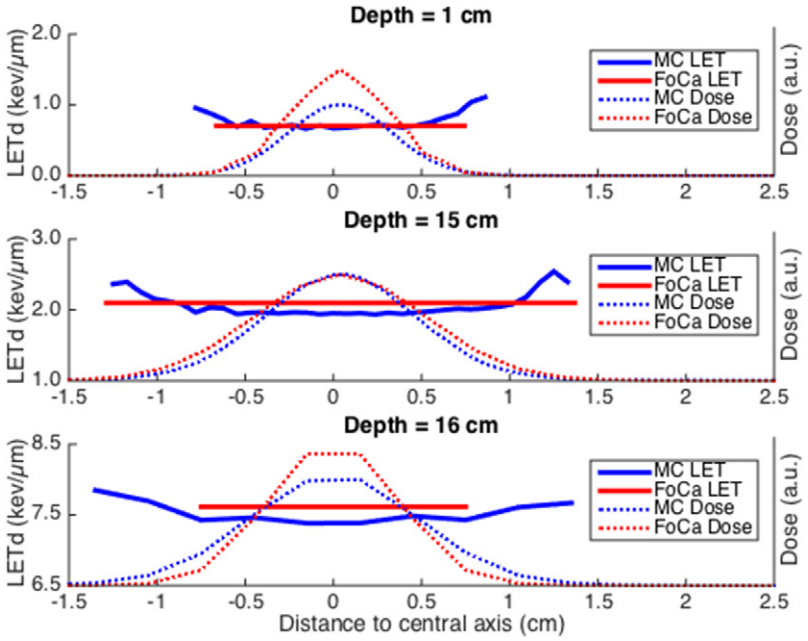


**Figure 2.** Transversal dose and LET profiles, calculated with Monte Carlo and FoCa, for a monoenergetic proton beam with $R = 16\,\text{cm}$ (at three different depths: $z = 1\,\text{cm}$, $z = 15\,\text{cm}$ and $z = 16\,\text{cm}$). Note the different $Y$ scales in the three plots.

## 3. Results

### *3.1. Pencil beams*

The irradiation of five mono-energetic, single-spot proton beams (with nominal ranges of 10, 13, 16, 19 and 22 cm and their corresponding clinical spot sizes, ranging between 0.7–1.1 cm FWHM in air at isocenter) in a water phantom was simulated with FoCa for dose and LET, using its *Robust* calculation algorithm and a calculation grid spacing of 2.5 mm in the transversal plane and 1 mm in the beam direction. The longitudinal (figure 1) and transversal (figure 2) LET profiles were compared against Monte Carlo data, showing a good agreement (except for some random noise in the very low dose areas of the Monte Carlo curves), with more than 98% of the FoCa LET values within 5% of the MC data. The bottom part of figure 1 shows how the secondary correction in FoCa accounts for the increased LET originating from secondary particles, which amounts to as much as 50% of the proton LET throughout the entrance channel.

### *3.2. Broad fields in a water phantom*

In the water phantom, we created two different pencil beam scanning (PBS) plans with a spherical target ($r = 3\,\text{cm}$), centered at a depth of 10 cm. The first plan (named *SPHERE 1F*) used a single field, while the second plan (*SPHERE 2F*) used two opposing fields on a $20 \times 20 \times 20\,\text{cm}$ cubic phantom. LET and dose profiles with FoCa and Monte Carlo were extracted for both plans and are shown in figure 3. The comparison of the longitudinal profiles (figure 3, top row) both follow the same trend: at phantom entrance, the LET is reproduced

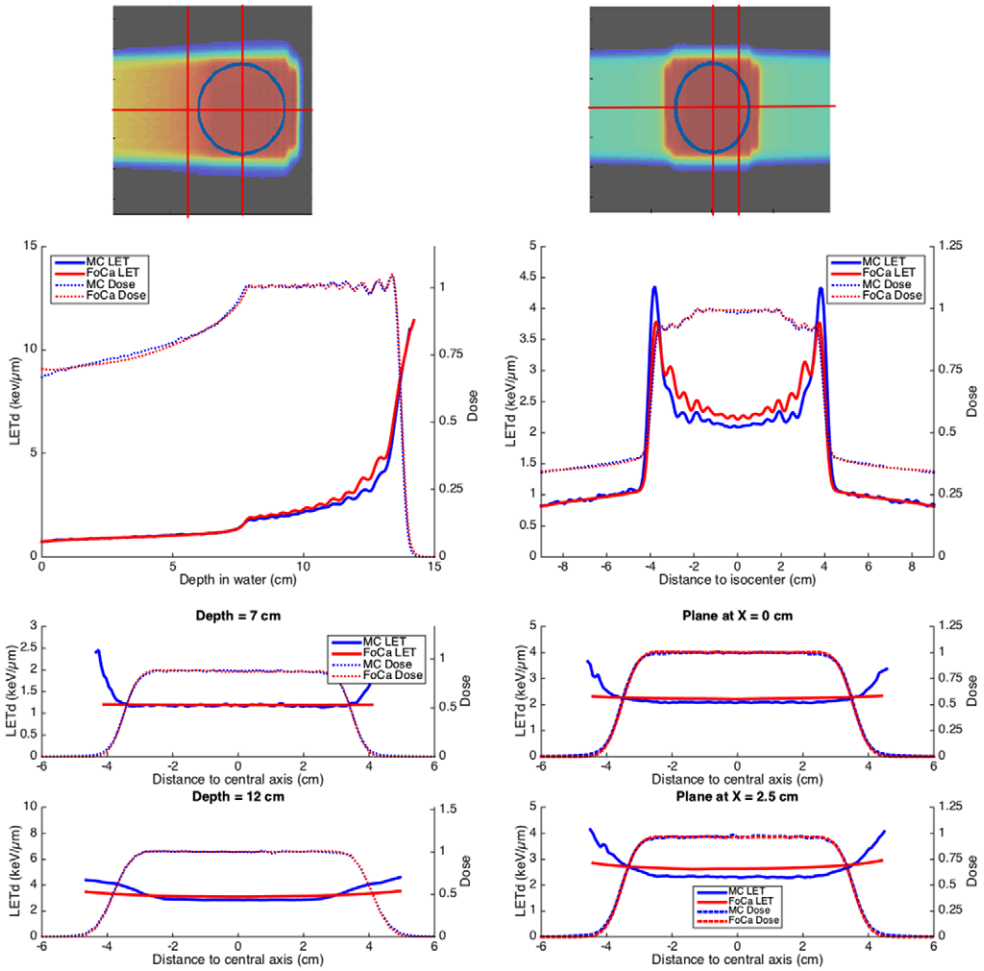


**Figure 3.** Longitudinal and transversal dose and LET profiles, calculated with Monte Carlo and FoCa, for scanned beams in a homogeneous water phantom using a single field (left) and two opposing fields (right) on a spherical target. The marked lines on the dose distributions (top) indicate the position of the profiles.

almost perfectly by the FoCa models, while towards the end of the range, increasing at the distal area of the spread-out Bragg peaks (SOBPs), there is a slight overestimation of the LET of about 0.5 keV $\mu$m$^{-1}$. This is caused by the physical approximation of the local energy spectra as a Gaussian function, which holds for the phantom entrance area but not when the particles approach the end of their range. When only a single energy is used (i.e. in pencil beams), this approximation affects equally the $\langle S^2 \rangle$ and $\langle S \rangle$ distributions, minimizing its final influence in the LET profiles; however, when both $\langle S^2 \rangle$ and $\langle S \rangle$ distributions are made up of different beamlets, the effect of the local energy spectrum approximation is no longer negligible.

The transversal profiles (figure 3, bottom rows) also show an interesting effect: the apparent LET increases in the penumbral areas, creating 'horns' in the transversal LET profiles. This effect is consistent with what was observed by Wilkens and Oelfke (2004) in their calculations for primary protons, and by Grassberger and Paganetti (2011) for secondary protons. It is caused by two processes: the natural divergence of the beam (which is included in the

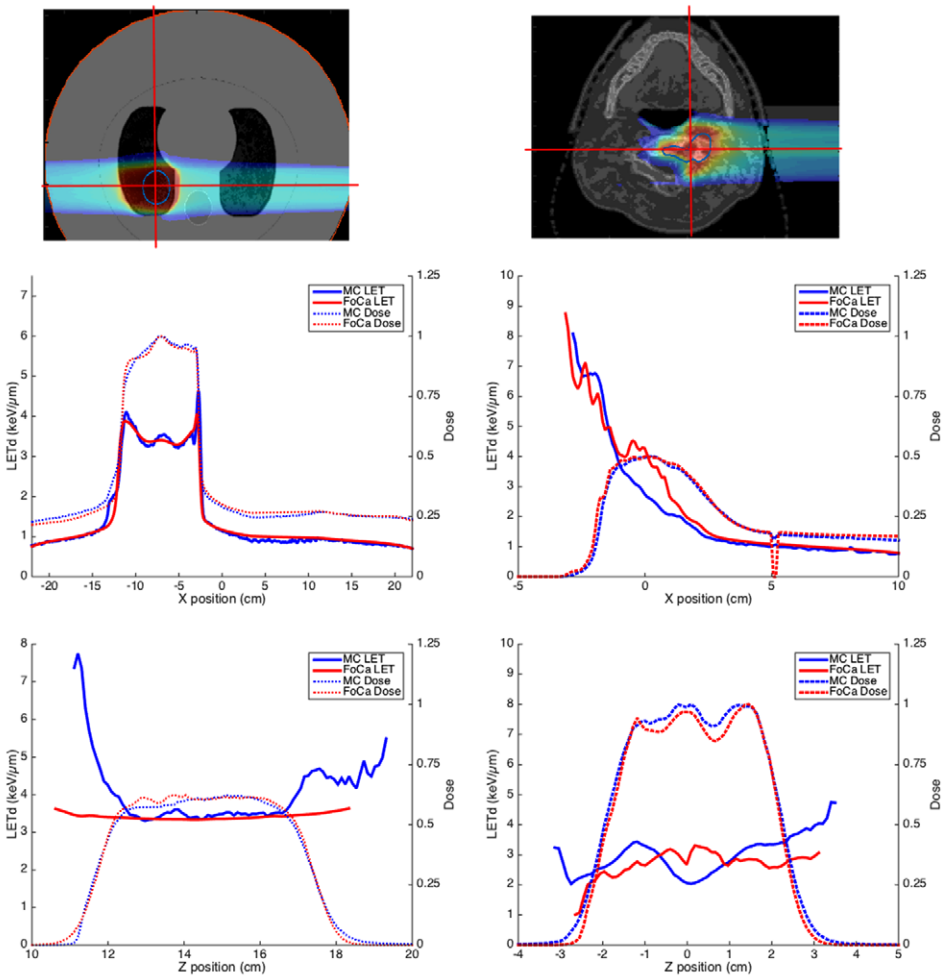


**Figure 4.** Longitudinal and transversal dose and LET profiles at isocentre, calculated with Monte Carlo and FoCa, for a two-field plan on a thoracic phantom (left) and a two-field clinical head and neck tumor (right). The marked lines on the dose distributions (top) indicate the position of the profiles. Drop in FoCa dose around $X = 5$ cm (top-right image) is caused by artificially zeroing dose in voxels outside the body contour, for computational reasons.

FoCa calculation model, as can be seen in the small curvature of the transversal LET profiles), and the lower energy of the deflected protons (via either multiple Coulomb scattering or nuclear interactions) found in the penumbral zone, which have a higher LET. These effects are expected, since both the primary proton LET model and the secondary correction are 1D and thus cannot account for penumbral variations in LET.

### *3.3. Clinical fields*

In order to assess the impact of the model uncertainties in a clinical setup, we studied four PBS plans on patient geometries: a spherical lung tumor on a tissue-equivalent phantom (with high and low density tissue inserts), a H and N case with a highly inhomogeneous geometry,

**Table 2.** Mean dose and LET differences [MC – FoCa] for the two spherical-target plans on a water phantom (single field and two opposing fields), and for the four clinical plans under study, calculated over all voxels with a dose higher than 1% of the prescription.

| | Dose difference (% of prescription) | | LET Difference (keV $\mu$m$^{-1}$) | |
|---|---|---|---|---|
| | Mean | StDev | Mean | StDev |
| SPHERE 1F | −0.4 | 1.5 | −0.017 | 0.359 |
| SPHERE 2F | −0.4 | 1.1 | 0.010 | 0.336 |
| LUNG PH | −0.2 | 3.4 | −0.058 | 0.400 |
| PROSTATE | 0.6 | 4.0 | 0.014 | 0.281 |
| PEDIATRIC | −0.4 | 4.4 | −0.062 | 0.483 |
| H and N | 0.1 | 3.7 | −0.033 | 0.592 |
| Averages | −0.1 | 3.0 | −0.024 | 0.409 |

a prostate case, and a pediatric brain tumor. Longitudinal and transversal profiles of two example cases are shown in figure 4, corresponding to the best agreement observed (for the thoracic phantom) and the biggest discrepancy (for the H and N case). For the thoracic phantom (figure 4, left column), the profiles are very similar to the two-field plan on the water phantom: very good agreement on the longitudinal profile and a reasonable concordance on most of the transversal profile, with a greater penumbral increase in LET due to the low density of the lung inserts. For the head and neck case (figure 4, right column), however, the agreement is not so good, with differences up to 1–2 keV $\mu$m$^{-1}$ in the central area of the target. In the lateral profile, FoCa cannot reproduce the LET variations caused by tissue inhomogeneities that we do observe in the Monte Carlo curve.

### *3.4. Statistical analysis, confidence interval and effect of the secondary proton correction*

In order to integrate the information of all phantoms and clinical cases analyzed, we performed statistical analysis on all dose and LET distributions, considering only voxels with at least 1% of the prescription dose. The results are summarized in table 2. While the dose distributions showed excellent agreement between FoCa and Monte Carlo, the LET distributions showed a higher deviation (standard deviation of 0.4 keV $\mu$m$^{-1}$), but it was mostly of random nature, since the mean difference was only of 0.02 keV $\mu$m$^{-1}$. This was caused by a combination of the failure of the local energy spectrum Gaussian approximation and the lateral penumbra and by the effect of inhomogeneities in the patient geometries.

In order to derive a confidence interval for the FoCa calculations of LET, we divided the fields into two segments: the low-LET, corresponding to the entrance channel and having a reasonably good agreement, and the high-LET, which corresponds to terminal protons where the fluctuations of LET are higher. In figure 5, we show histograms of the relative LET difference (FoCa-LET) for all six cases analyzed, for the low and high LET intervals. We explored different thresholds for low versus high LET, and derived, for each of them and for all of the studied cases, confidence intervals spanning exactly 68.27% of the voxels (1 standard deviation) with dose above the 1%-threshold. As a result of this process we found an optimal threshold value at 1.7 keV $\mu$m$^{-1}$ and obtained the following 1-sigma confidence interval for the FoCa LET values:

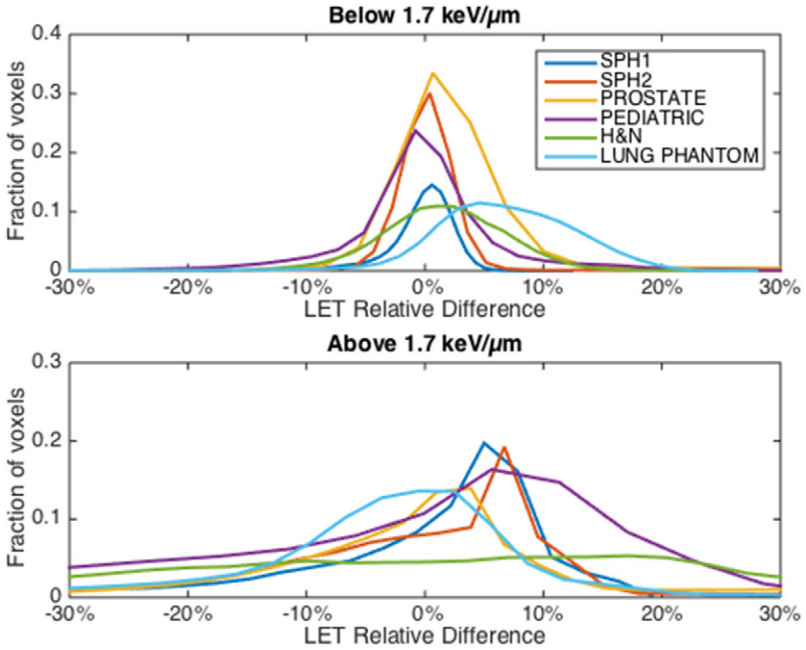


**Figure 5.** Histograms of relative difference in LET [MC – FoCa] for the two spherical-target plans on a water phantom (single field and two opposing fields), and for the four clinical plans under study, calculated over all voxels with a dose higher than 1% of the prescription, for low LET (above) and high LET (below) areas.

$$\partial\mathrm{LET} = \begin{cases} \pm 6\%, \ \mathrm{LET} \leqslant 1.7 \ \ \mathrm{keV} \ \mu\,\mathrm{m}^{-1} \\ \pm 22\%, \ \mathrm{LET} > 1.7 \ \ \mathrm{keV} \ \mu\,\mathrm{m}^{-1}. \end{cases} \tag{6}$$

Examples of the application on this confidence interval are depicted in figure 6. It is worth mentioning that, as expected, the discrepancies in LET calculation are higher in the low-dose areas, as evidenced by the dependence of size 1-sigma confidence interval with the dose threshold: $\partial$LET decreases to 5% for low-LET and 18% for high-LET areas when choosing a dose threshold of 5%, and further down to 5% / 16% when the dose threshold is 10%.

Dot-dashed lines on figure 6 also depict LET calculations both with FoCa and with Monte Carlo using only primary protons. These curves reflect how the secondary protons correction plays a role in the entrance channel area (as seen in the longitudinal profiles at the top, with differences up to 0.5 keV $\mu\mathrm{m}^{-1}$) but has a very limited impact on the peak area, as shown in the transversal profiles through isocentre, where both curves remain within 0.1 keV $\mu\mathrm{m}^{-1}$ of one another.

### *3.5. Derivation of radiobiological data from the LET of primary particles*

The confidence interval derived in the previous section was propagated to the dose-weighted RBE calculations, resulting in an average dose uncertainty of 3% in the target area (dose above 90% of prescription) and 2% elsewhere, with a maximum observed value of 5%. In other words, the obtained accuracy in the LET calculations allows us to derive RBE-weighted dose distributions based on phenomenological RBE models where the limiting factor is no

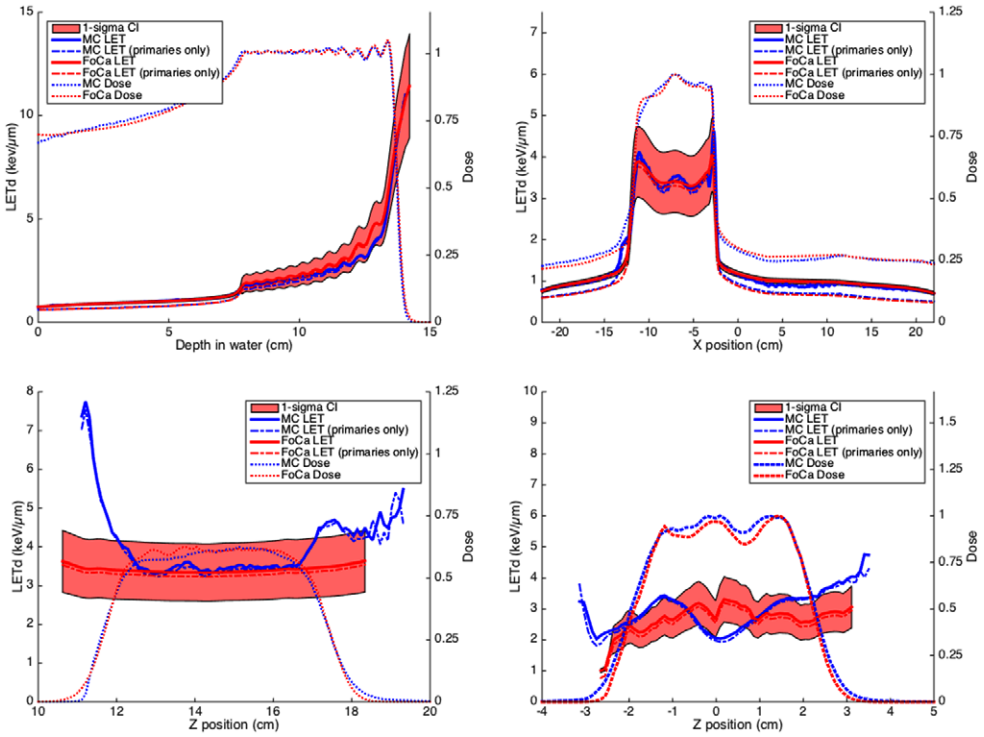


**Figure 6.** Different profiles through field isocentre showing dose, LET, and LET from primary protons only, calculated with FoCa and Monte Carlo, including the 1-sigma confidence interval derived in section 3.4 (top-left: longitudinal profile for single spherical-target field on water phantom; top-right: longitudinal profile on tissue-equivalent thoracic phantom; bottom-left: transversal profile on tissue-equivalent thoracic phantom; bottom-right: transversal profile on head and neck patient).

longer the uncertainty of the LET distributions, but rather, the RBE models themselves and the uncertainty of the $\alpha/\beta$ ratios.

The results of some representative RBE-weighted dose curves are shown in figure 7. There is a great similarity between the Monte Carlo values and the FoCa-predicted values in all cases, minimizing the influence of the discrepancies in the LET distributions. It is worth noting that the obtained values are, in some cases, significantly different from the standard value of 1.1 (Paganetti *et al* 2002, Paganetti 2014), which calls for a reflection on the convenience of using patient-specific, 3D distributions of RBE. This is even more evident in the RBE-weighed dose volume histograms (DVHs) depicted in figure 8; there is great overlap between the FoCa and MC curves, with the MC curves falling almost completely within the confidence interval (except for penumbral areas with very low dose, where the FoCa physical dose distributions deviates slightly from the Monte Carlo), and the RBE $= 1.1$ curves appear out of the confidence interval for significant parts of the target volumes. The very high LET areas visible, for example, in the top-left or bottom-left plots in figure 7 correspond to areas within the 90% isodose curve which lay outside the target: their $\alpha/\beta$ ratios are set at 3 Gy (compared to 10 Gy inside the target), which makes the RBE increase as given by equation (6). Since these areas are located just outside the target, they do not appear in the target curves from the biological DVHs in figure 8.

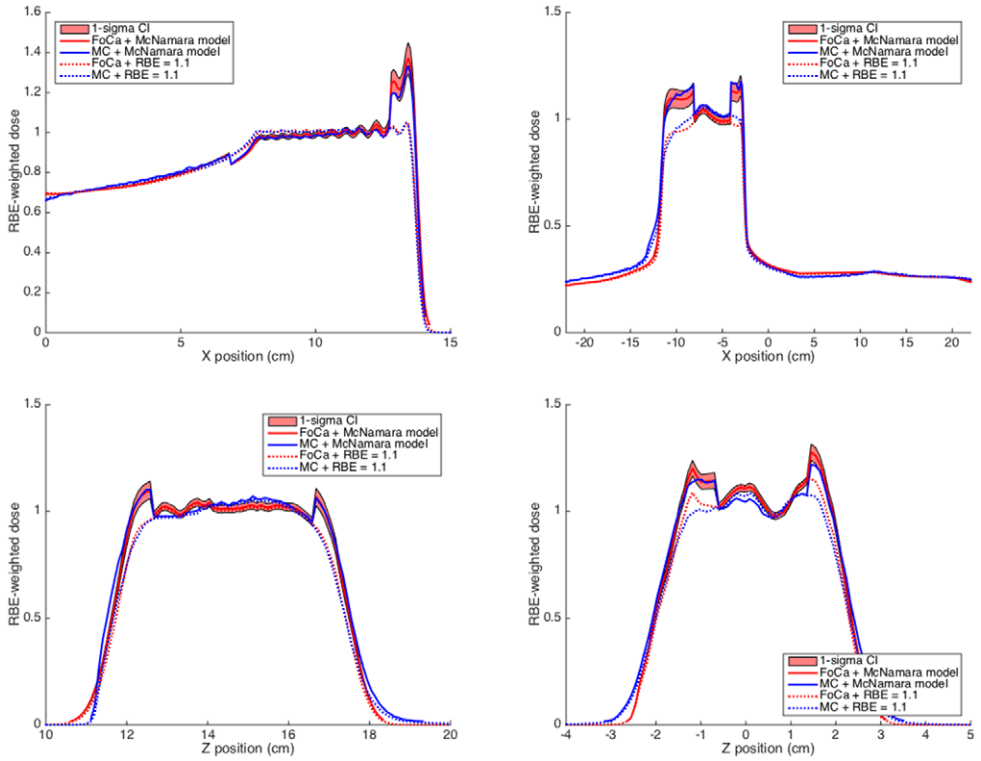


**Figure 7.** RBE-weighted dose calculated using McNamara model and dose and LET data from FoCa and Monte Carlo, for the four profiles depicted in figure 6, compared with the standard RBE-weighted dose calculated with a fixed RBE = 1.1. The 1-sigma confidence in RBE-weighted doses has been propagated to the equivalent interval in LET shown in figure 6 (ignoring the uncertainties in the dose and the $\alpha/\beta$ ratios), for illustrative purposes.

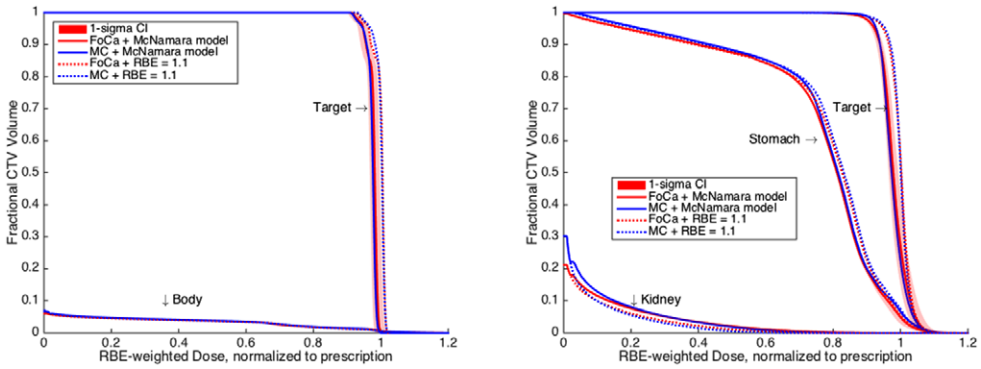


**Figure 8.** RBE-weighted dose volume histograms for the two-field uniform plan in the water phantom (left), and for the pediatric case (right), showing the propagated confidence interval from the LET calculation with FoCa. Horizontal axis shows RBE-weighted dose normalized to prescription.

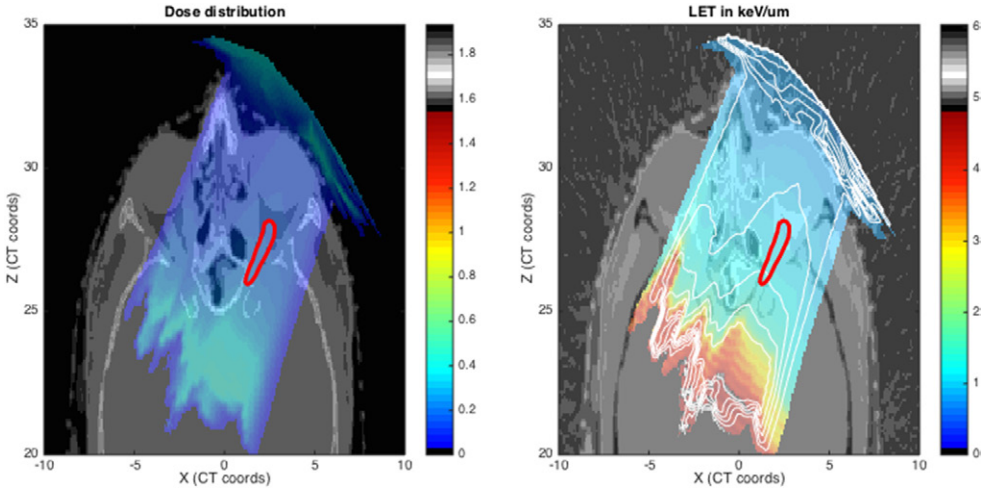


**Figure 9.** Physical dose relative to prescription (left) and LET distribution (right) for a lateral anterior oblique proton PBS field in a brain patient, calculated with FoCa. Line shows the contoured left optic nerve.

The effect of the new secondary proton LET model can also be assessed in terms of increased capability for calculating RBE and RBE-weighted doses based on the phenomenological models. The dose and LET calculations depicted in figure 9 show a case where variable RBE can lead to range uncertainties, a brain tumor treated with a lateral anterior oblique proton field, very similar to the one studied by Carabe *et al* (2012). The average LET in the left optic nerve region (contoured in the figure) was calculated with FoCa to be 0.96 keV $\mu$m$^{-1}$, using the new secondary model, while the same calculation with FoCa using only primary protons yielded a mean LET of 0.76 keV $\mu$m$^{-1}$. This discrepancy caused the obtained RBE-weighted dose (calculated with equation (5) and using an $\alpha/\beta$ value of 1.6 Gy for the optic nerve tissue) to be 4% lower (on average) when using the primary-only LET than when using the full calculation.

## 4. Discussion and conclusions

Coupling the 1D LET model and secondary correction with the convolution-superposition calculation algorithm in FoCa, we were able to produce fast LETd distributions in patient geometries. The full (dose + LET) calculation times were of the order of 3–5 min per field with the *Robust* algorithm (Sánchez-Parcerisa *et al* 2014b), with a non-precalculable, field-position specific time of under 1 second per field for the *Fast* algorithm, on a desktop iMac computer with a 3.1 GHz Intel Core i5 processor. While these times are still subject to further optimization, they are significantly faster than the average 1 day/field that we needed to perform the Monte Carlo calculations on our high performance cluster, using about 20 CPU cores per field and 100 000 primaries per spot.

While the object of this study was not to assess the validity of the dose calculations, which have been benchmarked already against commissioning data (Sanchez-Parcerisa *et al* 2014a), there is indeed a good agreement between the FoCa and the Monte Carlo doses. They are depicted in the plots as well as they can sometimes explain the deviations in LET; for instance, in figure 1, the small deviation in the LET curve present in the $R = 10$ cm beam

can be explained by an imperfect modeling of the Bragg peak straggling at low energies, as evidenced by the matching deviation in the corresponding longitudinal dose profile.

The accuracy of the calculations was remarkable for single proton beamlets, and reasonably good elsewhere. The secondary-particle correction, albeit simple, seems enough to predict the effect of secondary particles in the integrated distributions. Two main issues remain to be improved in further versions of the models: a refinement of the longitudinal energy spectra model, and the extension of the underlying models to include 3D effects, both for the primary particle model and for the secondary particle correction. Other effects studied in similar works, such as the effect of beam spot sizes in the secondary correction (Marsolat *et al* 2015), or the contribution of secondary fragments heavier than protons (Grassberger and Paganetti 2011, Romano *et al* 2014) are other issues worth investigating on further releases; however, the expected effect of these phenomena on the final LET values is much lower.

In the derivation of the 1-sigma confidence interval we neglected the possible uncertainty of the Monte Carlo calculation, which is discussed elsewhere (Grassberger and Paganetti 2011, Cortés-Giraldo and Carabe 2015, Granville and Sawakuchi 2015). We consider the uncertainties discussed in those references to be lower in magnitude than the discrepancies observed between our model and the Monte Carlo calculated LETs, and thus perfectly included in the derived confidence interval. Also, we derived these intervals using a conservative low dose threshold of 1%. It may be worth investigating raising this threshold, in terms of the clinical relevance of a possibly increased radiobiological effectiveness of such low-dose areas, in order to obtain a more accurate confidence interval for the LET. Additionally, another possibility is to derive different confidence intervals for different dose levels.

The application of the FoCa dose/LET calculation models with a phenomenological RBE calculation model brings up the possibility of calculating radiobiological doses on the fly during treatment planning, and possibly performing radiobiological optimization. After our implementation of fast LET calculation, the limiting factor for these RBE estimations is no longer the LET calculation, but the uncertainty of the $\alpha/\beta$ ratios and of the RBE models themselves. A thorough and straightforward uncertainty analysis, including all the components of each of the models, is vital to be able to switch from using a constant value of proton RBE to a full calculation of biological doses.

## Funding

This work was supported in part by Varian Medical Systems, Inc. through a Master Research Agreement with the University of Pennsylvania, and by the Spanish Ministry of Economy and Competitivity grant FPA2014-53290-C2-2-P.

## References

Agostinelli S *et al* 2003 GEANT4—a simulation toolkit *Nucl. Instrum. Methods Phys. Res.* A **506** 250–303

Bortfeld T 1997 An analytical approximation of the Bragg curve for therapeutic proton beams *Med. Phys.* **24** 2024–33

Carabe-Fernandez A *et al* 2007 The incorporation of the concept of minimum RBE (RBE min) into the linear-quadratic model and the potential for improved radiobiological analysis of high-LET treatments *Int. J. Radiat. Biol.* **83** 27–39

Carabe A *et al* 2012 Range uncertainty in proton therapy due to variable biological effectiveness *Phys. Med. Biol.* **57** 1169

Carabe A *et al* 2013 Clinical consequences of relative biological effectiveness variations in proton radiotherapy of the prostate, brain and liver *Phys. Med. Biol.* **58** 2103
Cortés-Giraldo M A and Carabe A 2015 A critical study of different Monte Carlo scoring methods of dose average linear-energy-transfer maps calculated in voxelized geometries irradiated with clinical proton beams *Phys. Med. Biol.* **60** 2645
Dasu A and Toma-Dasu I 2012 Prostate alpha/beta revisited-an analysis of clinical results from 14 168 patients *Acta Oncol.* **51** 963–74
Dolney D *et al* 2013 Dose perturbations by electromagnetic transponders in the proton environment *Phys. Med. Biol.* **58** 1495–505
Fager M *et al* 2015 Linear energy transfer painting with proton therapy: a means of reducing radiation doses with equivalent clinical effectiveness *Int. J. Radiat. Oncol. Biol. Phys.* **91** 1057–64
Ferrari A *et al* 2005 FLUKA: a multi-particle transport code, CERN-2005–10, INFN/TC_05/11, SLAC-R-737
Giantsoudi D *et al* 2013 Linear energy transfer-guided optimization in intensity modulated proton therapy: feasibility study and clinical potential. *Int. J. Radiat. Oncol. Biol. Phys.* **87** 216
Granville D A and Sawakuchi G O 2015 Comparison of linear energy transfer scoring techniques in Monte Carlo simulations of proton beams *Phys. Med. Biol.* **60** N283–91
Grassberger C and Paganetti H 2011 Elevated LET components in clinical proton beams *Phys. Med. Biol.* **56** 6677
Grassberger C *et al* 2011 Variations in linear energy transfer within clinical proton therapy fields and the potential for biological treatment planning *Int. J. Radiat. Oncol. Biol. Phys.* **80** 1559–66
Guardiola C *et al* 2015 Preliminary microdosimetric measurements with ultra-thin 3D silicon detectors of a 62 MeV proton beam *J. Instrum.* **10** P01008
ICRU 1998 Fundamental quantities and units for ionizing radiation. *International Commission on Radiation Units and Measurements Technical Report 60* (Bethesda, MD: ICRU)
Jarlskog C Z and Paganetti H 2008 Physics settings for using the Geant4 toolkit in proton therapy *IEEE Trans. Nucl. Sci.* **55** 1018–25
Kase Y *et al* 2012 Microdosimetric calculation of relative biological effectiveness for design of therapeutic proton beams *J. Radiat. Res.* **54** 485–93
Kehwar T S and Sharma S C 2003 Use of normal tissue tolerance doses into linear quadratic equation to estimate normal tissue complication probability *Radiat. Oncol.* (http://www.rooj.com/Radiation%20Tissue%20Tolerance.htm)
Kraft G and Kramer M 2013 Linear energy transfer and track structure *DNA and Chromatin Damage Caused by Radiation* ed J T Lett and W K Sinclair (New York: Academic)
Marsolat F *et al* 2015 Analytical model for LET calculations along protons Pencil Beam axis. PTCOG 54, San Diego, CA, P114
McNamara A L *et al* 2015 A phenomenological relative biological effectiveness (RBE) model for proton therapy based on all published *in vitro* cell survival data *Phys. Med. Biol.* **60** 8399
Paganetti H *et al* 2002 Relative biological effectiveness (RBE) values for proton beam therapy *Int. J. Radiat. Oncol. Biol. Phys.* **53** 407–21
Paganetti H 2012 Range uncertainties in proton therapy and the role of Monte Carlo simulations *Phys. Med. Biol.* **57** R99
Paganetti H 2014 Relative biological effectiveness (RBE) values for proton beam therapy. Variations as a function of biological endpoint, dose, and linear energy transfer *Phys. Med. Biol.* **59** R419
Paul H and Sanchez-Parcerisa D 2013 A critical overview of recent stopping power programs for positive ions in solid elements *Nucl. Instrum. Methods Phys. Res.* B **312** 110
Pérez-Andujar A *et al* 2012 Microdosimetric measurements for neutron-absorbed dose determination during proton therapy *Radiat. Prot. Dosim.* **151** 365–73
Rollet S *et al* 2011 Microdosimetric assessment of the radiation quality of a therapeutic proton beam: comparison between numerical simulation and experimental measurements *Radiat. Prot. Dosim.* **143** 445
Romano F *et al* 2014 A Monte Carlo study for the calculation of the average linear energy transfer (LET) distributions for a clinical proton beam line and a radiobiological carbon ion beam line *Phys. Med. Biol.* **59** 2863
Rosenfeld A *et al* 2000 New silicon detector for microdosimetry applications in proton therapy *IEEE Trans. Nucl. Sci.* **47** 1386–94
Sanchez-Parcerisa D *et al* 2014a FoCa: a modular treatment planning system for proton radiotherapy with research and educational purposes *Phys. Med. Biol.* **59** 7341

Sanchez-Parcerisa D *et al* 2014b Fast range switching of passively scattered proton beams using a modulation wheel and dynamic beam current modulation *Phys. Med. Biol.* **59** N19
Sanchez-Parcerisa D *et al* 2012 Influence of the delta ray production threshold on water-to-air stopping power ratio calculations for carbon ion beam radiotherapy *Phys. Med. Biol.* **58** 145
Schaffner B 2008 Proton dose calculation based on in-air fluence measurements *Phys. Med. Biol.* **53** 1545–62
Ulmer W and Schaffner B 2011 Foundation of an analytical proton beamlet model for inclusion in a general proton dose calculation system *Radiat. Phys. Chem.* **80** 378–89
Wedenberg M *et al* 2013 A model for the relative biological effectiveness of protons: the tissue specific parameter $\alpha/\beta$ of photons is a predictor for the sensitivity to LET changes *Acta Oncol.* **52** 580–8
Wilkens J J and Oelfke U 2003 Analytical linear energy transfer calculations for proton therapy *Med. Phys.* **30** 806–15
Wilkens J J and Oelfke U 2004 Three-dimensional LET calculations for treatment planning of proton therapy *Z. Med. Phys.* **14** 41–46
Wroe A *et al* 2009 Out-of-field dose equivalents delivered by passively scattered therapeutic proton beams for clinically relevant field configurations *Int. J. Radiat. Oncol. Biol. Phys.* **73** 306–13